

SuperFront: From Low-resolution to High-resolution Frontal Face Synthesis

Yu Yin, Joseph P. Robinson, Songyao Jiang, Yue Bai, Can Qin, Yun Fu

Department of Electrical and Computer Engineering
Northeastern University, Boston, MA

{yin.yul, robinson.jo, jiang.so, bai.yue, qin.ca}@northeastern.edu, yunfu@ece.neu.edu

Abstract

Advances in face rotation, along with other face-based generative tasks, are more frequent as we advance further in topics of deep learning. Even as impressive milestones are achieved in synthesizing faces, the importance of preserving identity is needed in practice and should not be overlooked. Also, the difficulty should not be more for data with obscured faces, heavier poses, and lower quality. Existing methods tend to focus on samples with variation in pose, but with the assumption data is high in quality. We propose a generative adversarial network (GAN)-based model to generate high-quality, identity preserving frontal faces from one or multiple low-resolution (LR) faces with extreme poses. Specifically, we propose SuperFront GAN (SF-GAN) to synthesize a high-resolution (HR), frontal face from one-to-many LR faces with various poses and with the identity-preserved. We integrate a super-resolution (SR) side-view module into SF-GAN to preserve identity information and fine details of the side-views in HR space, which helps model reconstruct high-frequency information of faces (i.e. periocular, nose, and mouth regions). Moreover, SF-GAN accepts multiple LR faces as input, and improves each added sample. We squeeze additional gain in performance with an orthogonal constraint in the generator to penalize redundant latent representations and, hence, diversify the learned features space. Quantitative and qualitative results demonstrate the superiority of SF-GAN over others.

1. Introduction

Face-based generative tasks (e.g. face rotation [13, 16, 34, 40], hallucination [3, 4, 41], and attribute editing [5, 12]) have gained more of the spotlight in research communities with the advancement of deep learning. Even still, the practical significance of identity-preservation is frequently overlooked, which is especially a challenge for faces with larger pose and lower quality. Recently, some progress has been made to synthesize frontal faces with large pose variations [16, 22, 26]. However, existing methods fo-

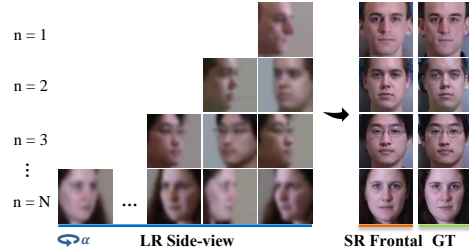


Figure 1: **Single-to-many input capability.** SF-GAN takes N LR, side-view faces, of arbitrary angle (α), as input. The proposed synthesizing high-quality frontal faces from one input, then improves with more added.

cus on faces with large poses, while assuming images are high in quality - previous attempts lose identity information when learning a highly non-linear transformation that maps spaces of low-resolution (LR) side-views to high-resolution (HR) frontal-views.

Both low quality inputs and large pose discrepancy between views make the frontalization problem challenging. Modern-day models usually aim to solve either of the challenges (i.e. face super-resolution (SR) [4, 3] or large pose face frontalization [16, 40]), but then breakdown when faces are both low quality and large poses. To overcome these barriers, simultaneously, we proposed SuperFront GAN (SF-GAN). Hence, SF-GAN synthesizes HR and identity-preserved frontal face from an LR face with an arbitrary pose. For this, a SR module is integrated into SF-GAN to preserve the identity for low-quality of images. Following this, a patch loss is introduced to solve large pose discrepancies by learning a precise non-linear transformations from LR side-views to HR frontal. Furthermore, we believe that the information in a single LR image under extreme poses is limited (i.e. insufficient for synthesizing accurate frontal faces in extreme cases). Hence, we designed the model to accept one-to-many inputs - each added sample further improve the results. A discussion of the three challenges, along with the proposed solutions, is presented for each.

Existing face frontalization methods [13, 16, 22, 39] tend

to set the generator as an encoder-decoders with skip connections (*i.e.* U-Net [29]). This preserves low-frequency information (*i.e.* shape and uniqueness of objects) by skip connections, while cascades of convolutional-layers learn high-frequency features. However, precise low-frequency information is lost when faced with LR inputs. Thus, U-Net architectures lead to inaccuracies at inference in such cases (*e.g.* blurred structures and loss of identity). To properly preserve details and the subject identity of LR face, we leverage a super-resolution (SR) module in parallel to better provide precise low-frequency information and high-frequency details. The effectiveness of the proposed joint-learning scheme is met with improved quality of high-frequency content, while preserving the identity of the subject. To the best of our knowledge, we are the first to address the problem of rotating profile faces and SR jointly, and such that the tasks compliment one another.

Another challenge in frontal face synthesis is the highly non-linear transformation from side-to-front view due to large pose discrepancy, leading to imprecise facial structures at inference. Previous works [16, 22, 34] usually use pixel-level (*e.g.* L1 or L2), identity, and adversarial losses to learn mappings between views. However, models trained such losses typically have low confidence in differentiating structural information [16, 27]. To capture detailed facial structures as well as identity information of the subject, we incorporate an patch-level loss into the commonly used loss set (*i.e.* pixel loss, identity loss, and adversarial loss), and hence, reinforce the model to pay more attention to image structures (*i.e.* the edge and shape of facial components), (*i.e.* Structural Similarity Index (SSIM) [35]). Different from existing works, we add structure-level knowledge in the form of complimentary information provided on the patch-level, showing a significant boost in the final result. We show the effectiveness of the patch-based loss in ablation study.

Moreover, synthesizing HR and identity preserving frontal views from a single image is often difficult due to extreme poses in LR faces. In many real-life scenarios (*e.g.* surveillance system), there are multiple images per subject that can be used in a complimentary fashion to further improve the synthesis [34]. However, most existing face frontalization algorithms only handle one image at each time. To further boost the quality of the face, we extend our model to accept multiple faces as input (Fig. 1). Since all generators in the proposed model share the same weights, the input image could have arbitrary poses. Instead of employing naive fusion methods (*e.g.* image- or feature-level concatenation [28], or feature-level summation [34]), we propose using orthogonal regularization in our generative adversarial network (GAN)-based model for optimal training and to learn features of broader span [2]. To the best of our knowledge, we are the first to introduce this in training

a GAN-based model. Namely, SF-GAN.

In summary, we make the following contributions:

1. To our best knowledge, we are the first to tackle the challenge of tiny face frontalization by proposing a multi-tasking model which learns the frontalization and face super-resolution collaboratively.
2. We introduce a patch-based loss to capture facial structures and learn a precise non-linear transformation between LR side-view and HR frontal-view faces.
3. We extend one-to-multiple inputs: more LR inputs better preserve identity and improve synthesis quality using early or late fusion. Furthermore, we add constraints to diversify the features (*i.e.* orthogonal regularization) for more improvement.

2. Related Work

2.1. Generative adversarial network

Introduced in [8], GAN train by facing generator (G) off against discriminator (D) in a *min-max* game, where G aims to generate images indistinguishable from *real* x from noise z (*i.e.* $G(z) \rightarrow \tilde{x}$, where \tilde{x} is generated version of x). Recently, GAN have been successfully applied to various tasks like image-to-image translation [17], image super-resolution [21], and image in-painting [25]. These successful applications of GAN motivate us to develop super-resolved frontal face synthesis methods based on GAN.

2.2. Face frontalization

Face frontalization is a challenging task due to incomplete information in face images when captured from a side-view. Previous attempts at the problem can be characterized in two fold: traditional (*i.e.* *shallow*) methods and deep learning approaches. Traditional methods include 3D Morphable Model (3DMM) based methods [1, 23, 20] and statistical-based models [34, 30]. We focus the remainder of the literature review on the more relevant, state-of-the-art deep learning works [19, 34, 39, 45, 46, 44].

Most similar to the proposed are GAN-based frontal-face synthesizers [6, 16, 33, 34]. BiGAN jointly learns G and an inference model [6]. Nonetheless, in practice, BiGAN produces poor quality due to finite data and limited model capacity [34]. Like us, DR-GAN [34] learned identity-preserved representations to synthesize multi-view images. However, the encoder feeds the decoder, which depends on the training data— an impractical restriction for the inability to generalize to new data. TP-GAN has two pathways for frontal face generation to captured local and global features [16]. CR-GAN [33] also had dual paths, with the addition of self-supervision to refine weights learned by the

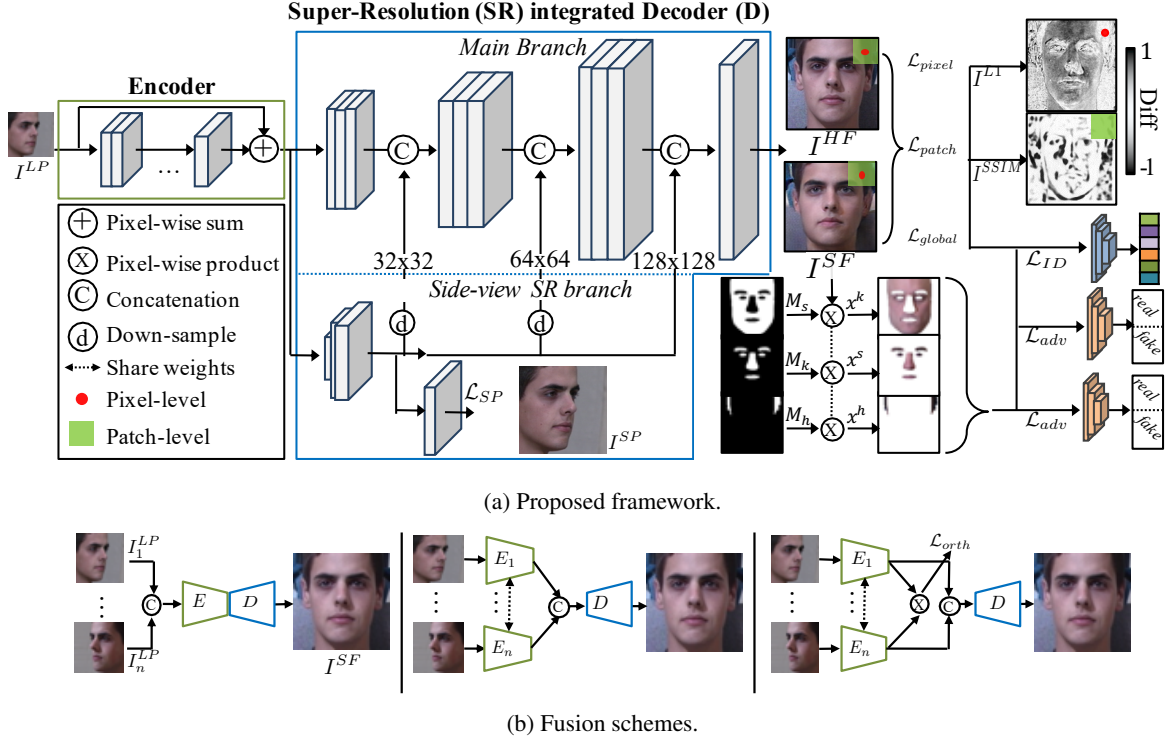


Figure 2: **Framework Overview.** (a) Given a non-frontal (*i.e.* profile) LR face I^{LP} , SI SF-GAN synthesizes a high-quality frontal face I^{SF} by integrating a side-view SR. (b) Furthermore, the proposed generalizes to multi-images of arbitrary poses as inputs—each added sample improves results. Our MI SF-GAN, even by naively fusing image inputs ((b) left), consistently outperforms SI in quality and identity preservation. Results are again boosted, drastically in fact (Table 5), by fusing features after the encoder ((b) middle). Constraints force diverse features ((b) right); again, yielding a boost.

supervised module. We, too, look at various levels, including the addition of patch-level and enhanced global loss. FF-GAN [39] adopted the 3DMM conditioned on a GAN as facial prior knowledge. Finally, the work [22] introduced the Multi-yaw Multi-pitch high-quality database for Facial Pose Analysis (M²FPA). Benchmarks for the new data included many of the GAN-based methods reviewed above. The authors also introduced an sufficient parsing guided D, which we too incorporate in our model (Section 3.3).

2.3. Orthogonal regularization

Orthogonal regularization forces the feature space to be more diverse. For this, some add a hard orthogonality constraint via singular value decomposition to remain on a Stiefel manifold [32]. More recently, a *softer* variant was proposed, *i.e.* orthogonality regularization via Gram matrix per weight matrix to force a near identity matrix by the spectral [2] or Frobenius [37] norm: the former claims superiority with consistent improvements for Convolutional neural network (CNN) with novel regularization scheme, Spectral Restricted Isometry Property (SRIP). SRIP proved to generalize well, and by an ease-of-use. Having showed such

improvements in feed-forward CNN trained for classification, we extend SRIP to a GAN (*i.e.* SF-GAN).

3. Methodology

We next define the face-frontalization problem from a single LR image. Then, we describe the model and loss function of *single-image* (SI) SF-GAN. Finally, we introduce *multi-image* (MI) SF-GAN as an extension.

3.1. Problem formulation

Let $\{I^{HF}, I^{LP}\}$ be a pair of HR frontal and LR side-view faces. Given a side-view face I^{LP} , the goal is to train a generator G to synthesize the corresponding HR frontal face image $\hat{I}^{HF} = G(I^{LP})$ with identity-preserved in I^{HF} .

A depiction of the general architecture of the proposed SF-GAN is in Fig. 2. G contains a deep encoder, a side-view SR module, and a decoder. SR of side-view imagery is integrated into SF-GAN to provide fine details of side-view faces, and hence help reconstruct higher frequency information (*i.e.* periocular, nose, and mouth regions) of frontal faces. Except for the novel architecture, we make

this SR and ill-posed problem well constrained by introducing a three-level loss (*i.e.* pixel-, patch-, and global-based losses) that learns a precise non-linear transformation between LR side-view and HR frontal-view faces.

3.2. Network architecture

The generator G contains a deep encoder, while the decoder contains a SR module. Features extracted by the deep encoder are passed to the SR-branch for reconstruction. The SR side-view module feeds the decoder with higher frequency information to help reconstruct frontal faces. See supplemental material for all network specifications.

Deep encoder. Previous works in face rotation often employ U-Net-like models [29]. We argue that the usual encoder is too shallow to capture the high-frequency information needed to recover a high-quality, HR face from LR space. Instead, we adopt a deeper encoder to recover edges and shapes of the HR frontal faces with higher precision. Another benefit is easing the task of SR of a side-view LR image, which provides details needed for reconstructing a HR frontal face. The encoder is shown in Fig. 2: a 3×3 conv-layer followed by sixteen residual dense blocks [43].

SR-integrated decoder. From the output of the encoder, the two branches split, the side-view SR module to super-resolve side-view images and, ultimately, pass feed back into the main path, along with the decoder that reconstructs HR frontal faces (Fig. 2). The *side-view SR* uses pixel shuffle to up-sample [31] by a factor of 4 (*i.e.* 128×128). From this, higher frequency content is fed to the main branch at various sizes to help reconstruct frontal faces.

3.3. Loss function

Pixel-level loss. L1 loss is used as a pixel-level loss, since it provides better convergence than L2 in supervised image generation tasks. We adopt pixel-wise L1 loss to measure both super-resolved side-view faces I^{SP} and synthesized frontal faces I^{SF} :

$$\mathcal{L}_{pix} = \frac{1}{W \times H} \sum_{w,h=1}^{W,H} |I_{w,h}^{HP} - I_{w,h}^{SP}| + |I_{w,h}^{HF} - I_{w,h}^{SF}|, \quad (1)$$

where W and H are the width and height of synthesized images (*i.e.* 128×128), respectively. I^{HP} and I^{HF} denote HR side-view and HR frontal faces, respectively.

Patch-level loss. Comparing to pixel-level loss, patch-level loss pays more attention to image structures (*i.e.* the edge and shape of facial components). Here we adopted SSIM [35] as patch-level loss to capture structural information and compliment pixel-level loss. SSIM measures the perceptual difference between a generated and a reference image. Let $\mathbf{x} = \{x_1, \dots, x_{K^2}\}$ and $\mathbf{y} = \{y_1, \dots, y_{K^2}\}$ be the pixel values of two corresponding $K \times K$ patches cropped from the synthesized I^{SF} and the HR frontal face I^{HF} , respectively.

The SSIM of \mathbf{x} and \mathbf{y} is computed as

$$SSIM(\mathbf{x}, \mathbf{y}) = 1 - \frac{(2\mu_x\mu_y + C_1)(2\sigma_{xy} + C_2)}{(\mu_x^2\mu_y^2 + C_1)(\sigma_x^2 + \sigma_y^2 + C_2)}, \quad (2)$$

where μ_x , μ_y and σ_x , σ_y corresponds to the mean and standard deviation of \mathbf{x} and \mathbf{y} , respectively. And σ_{xy} is the covariance of \mathbf{x} and \mathbf{y} . Constraints $C_1 = 0.01^2$ and $C_2 = 0.03^2$ are added for numeric stability.

Then, the patch-level loss is defined over P patches as

$$\mathcal{L}_{patch} = \frac{1}{P} \sum_{p=1}^P SSIM(\mathbf{x}^p, \mathbf{y}^p). \quad (3)$$

Global-level loss. In the global-level are adversarial and identity-preserving losses to synthesize photo-realistic frontal faces with high-frequency details and consistent identity as the input.

Adversarial loss. The frontal-face generative models should pay attention to all details used to distinguished a face as a whole to synthesize photo-realistic, frontal faces. Inspired by [22], we employ two discriminators at training (*i.e.* one for frontal faces D_f and another parsing-guided D_p). D_f aims to distinguish real HR frontal faces I^f from synthesized \hat{I}^f . D_p , although aims to work with D_f , focuses on different facial regions. Specifically, a pre-trained face parsing model [24] to generates images regions I^p to capture low-frequency information (*i.e.* skin regions), key-points (*i.e.* eyes, brows, nose, and lips), and hairline as

$$\begin{aligned} \text{real } I^p &= \{I^f \odot M_s, I^f \odot M_k, I^f \odot M_h\}, \\ \text{fake } \hat{I}^p &= \{\hat{I}^f \odot M_s, \hat{I}^f \odot M_k, \hat{I}^f \odot M_h\}. \end{aligned} \quad (4)$$

where M_s, M_k, M_h are skin, key-points, and hairline masks (Fig. 2). \odot is the element-wise product.

Then, the overall adversarial loss can be expressed as

$$\mathcal{L}_{adv} = \sum_{j \in \{f,p\}} \left(\mathbb{E}_{I^j} [\log D_j(I^j)] + \mathbb{E}_{\hat{I}^j} [\log(1 - D_j(\hat{I}^j))] \right). \quad (5)$$

Identity preserving loss. A critical aspect of evaluating face frontalization is the preservation of identities during the synthesis of frontal faces. We exploit the ability of pre-trained face recognition networks to extract meaningful feature representations to improve the identity preserving ability of G. Specifically, we employ a pre-trained 29-layer Light CNN¹ [36] with its weights fixed during training to calculate an identity preserving loss for G. The identity preserving loss is defined as the feature-level difference in the

¹Downloaded from <https://github.com/AlfredXiangWu/LightCNN>.

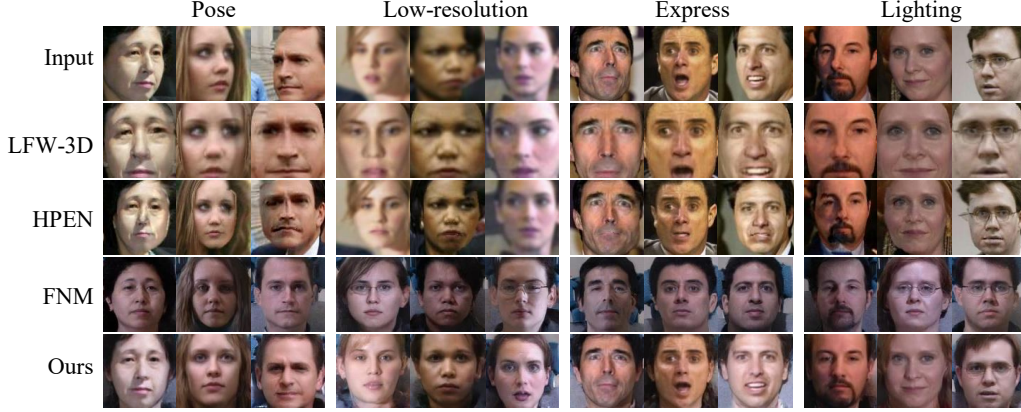


Figure 3: **Qualitative results on LFW [15]**. Comparison with SOTA under extreme pose, LR, expression, and lighting.

last two fully connected layers of Light CNN between the synthesized image I^{SF} and the ground-truth I^{HF} :

$$\mathcal{L}_{ID} = \sum_{i=1}^2 \|p_i(I^{SF}) - p_i(I^{HF})\|_2^2 \quad (6)$$

where $p_i (i \in 1, 2)$ denotes the outputs of the two fully connected layers of LightCNN, and $\|\cdot\|_2$ denotes the L2-norm.

Overall loss. The objective function for the proposed is a weighted sum of aforementioned three-level losses:

$$\mathcal{L}_G = \lambda_1 \mathcal{L}_{pix} + \lambda_2 \mathcal{L}_{patch} + \lambda_3 \mathcal{L}_{adv} + \lambda_4 \mathcal{L}_{ID} + \lambda_5 \mathcal{L}_{tv}, \quad (7)$$

where $\lambda_1, \lambda_2, \lambda_3, \lambda_4$, and λ_5 are hyper-parameters that control the trade-off of the loss terms. A total variation regularization \mathcal{L}_{tv} [18] is also included to remove unfavorable artifacts in synthesized frontal faces I^{SF} .

3.4. Multi-image SF-GAN

SI SF-GAN synthesized a SR frontal face from one side-view image. Yet, we often have multiple images per subject in real-life scenario (*e.g.* surveillance system). To leverage the complimentary information of different poses, we propose MI SF-GAN that can penalize redundant latent representations and explore the maximum information of the LR images under arbitrary poses. To be specific, MI SF-GAN use the same decoder as SI SF-GAN, but multiple encoders with shared weights for different input images. The framework of MI SF-GAN is shown in Fig. 2b. Different from image-level and feature-level fusion, MI SF-GAN introduce a constrain (*i.e.* orthogonal regularization) on the features extracted from the encoder. The orthogonal constrain makes the features more diverse and hence compliment each other as much as possible. We augment the objective function of SI SF-GAN with the loss:

$$\mathcal{L}_{orth} = \frac{1}{N} \sum_{n=1}^N \|G(I_n^{LP})^\top G(I_n^{LP})\|_F^2, \quad (8)$$

where N is the number of LR input images. $\|\cdot\|_F^2$ denotes the squared Frobenius norm. Then the loss function for MI SF-GAN can be expressed as:

$$\mathcal{L}_{MI} = \mathcal{L}_G + \mathcal{L}_{orth}. \quad (9)$$

4. Experiment

We now demonstrate the effectiveness of SF-GAN for HR frontal face synthesis and pose-invariant representation learning. We show quantitative synthesis results of the SI and MI SF-GAN and compare with the state-of-the-art methods trained on both LR and SR inputs. Besides, we highlight the identity preserved by the proposed by quantitatively evaluate the face recognition performance. Finally, we do an ablation study as a deep-dive revealing the benefits of the SR-integrated architecture, different types of loss function, and the multi-view fusion method.

4.1. Settings

Datasets. We conduct experiments on the Multi-PIE [9] and CAS-PEAL-R1 [7] datasets. The Multi-PIE consists of 337 subjects involved in up to 4 sessions. Each session included 20 illumination levels, 15 poses (*i.e.* within $\pm 90^\circ$, with a step size of $\pm 15^\circ$), and six expressions (*i.e.* neutral, smile, surprise, squint, disgust, and scream). Per convention, two settings of Multi-PIE followed [38, 16, 13, 22].

Setting 1 emphasizes pose, illumination, and minor expression variations. Thus, we only include a single image sample per session (*i.e.* Session 1). There are 250 identities, with the first 150 set as the training set, which includes the 9 poses spanning $\pm 60^\circ$ and 20 illumination levels per subject. A frontal face, neutral in expression and illumination, of the other 100 identities makes-up the search gallery, with the remaining face samples of these subjects set as probes.

Setting 2 emphasizes pose, illumination, and session (*i.e.* time) variations. Samples contain faces with neutral expressions from all four sessions and of all 337 identities.

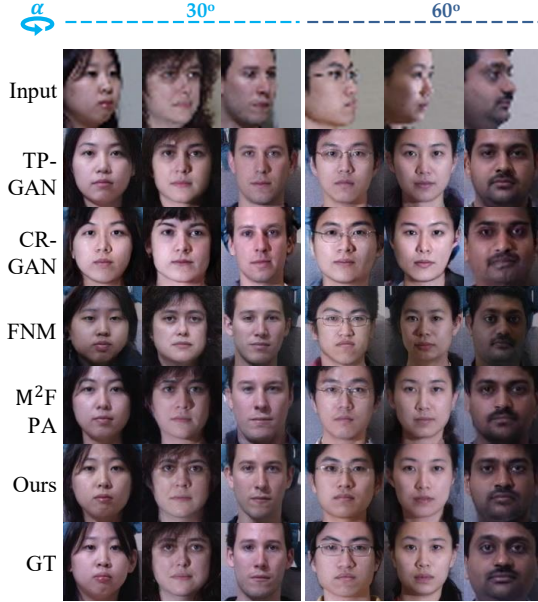


Figure 4: **Qualitative results on Multi-PIE.**

Samples of the first 200 identities are set as the training set; the remaining 137 subjects are used for testing, with, again, samples neutral in expression and illumination as the gallery. In total, there are 161,460, 72,000, and 137 faces for training, as test probes, and in the gallery, respectively. Notice, no overlap in subjects between train and test.

The CAS-PEAL-R1 dataset is a public large-scale face database made-up of pose, expression, accessory, and lighting variations. The dataset contains 30,863 grayscale pose images of 1,040 subjects, 595 males and 445 females, with 7 yaw angles within $\pm 45^\circ$ and 3 pitch angles within $\pm 30^\circ$, totaling to 21 yaw-pitch rotations. The training set is of all images for the first 600 subjects, and 440 for testing.

LFW [14] contains 13,233 face images collected in unconstrained environment. It will be used to evaluate the frontalization performance in uncontrolled settings.

Implementation. Training requires images pairs $\{I^{LP}, I^{HF}\}$, one LR side-view image and the corresponding HR frontal face. We first cropped images to a canonical view (128×128), making-up the HR images [16]. Then, LR images are created by bicubic downsampling ($4\times$). Unlike CAS-PEAL-R1, Multi-PIE is RGB. Thus, the identity-preserving model for Multi-Pie and CAS-PEAL-R1 were pre-trained on MS-Celeb-1M [10] in RGB and gray-scale, respectfully, and then fine-tuned on the respective training set. We implemented the model in PyTorch. Parameters were set as follows: $\lambda_1 = 20$, $\lambda_2 = 5$, $\lambda_3 = 0.8$, $\lambda_4 = 0.1$, $\lambda_4 = 1^{-4}$, $\lambda_3 = 0.1$. We used an ADAM optimizer with a learning rate of 10^{-4} , reducing 0.5 at 10^{th} and 15^{th} epochs for SI, and 5^{th} and 10^{th} epochs for MI (*i.e.* faster convergence). Batch of 8 for 20 epochs.

4.2. Face synthesis

In this section, we show results of the SI and MI SF-GAN, and compare with state-of-the-art methods. We used the public code of TP-GAN² [16], CR-GAN³ [33], and re-implemented M²FPA [22] since code is not public. For Multi-PIE, all the models were trained and evaluated for both settings (Section 4.1). Note that all synthesized results in paper were generated under *setting 2*. Fig. 4 (a) shows a qualitative comparison on Multi-PIE and demonstrates the superior performance of the proposed SF-GAN on LR images. Qualitative results show that the proposed SF-GAN can recover HR frontal faces from LR side-views with identity preserved and finer details (*i.e.* more precise facial shapes and textures). Notice other methods produce frontal faces with more inaccuracies due to blurry input.

We then demonstrate the robustness of SF-GAN to extreme pose, low-resolution, expression, and lighting. Fig. 3 shows the comparison results of SF-GAN and state-of-the-art methods (*i.e.* LFW-3D [11], HPEN [44], and FNM [26]) on the unconstrained dataset LFW [14]. More results on LFW will be provided in supplementary material.

Considering the other methods are designed for HR input and tend to fail learning the highly non-linear representation from LR side-view to HR frontal faces. We then quantitatively compare synthesis results of the state-of-the-art methods generated from super-resolved side-view faces for more fair comparison (see Table 1). We employ a pre-trained RCAN⁴ [42] as image SR model to generate super-resolved side-view images. Results are reported on PSNR and SSIM (Table 1) of synthesized frontal face. Quantitative results show that the proposed SI SF-GAN can not only achieve better results on LR input, but still recover frontal faces with better quality and finer structure than the state-of-the-art methods trained on SR input.

Fig. 5 shows the synthesized HR frontal results of both SI and MI SF-GAN with poses of 15° , 30° , 45° , 60° . Notice, photo-realistic faces are synthesized from one-to-many LR inputs of arbitrary views. The results for MI SF-GAN were from two LR inputs: the one used for the SI, and the other the inverted counterpart (*i.e.* $\pm 15^\circ$, $\pm 30^\circ$, $\pm 45^\circ$, $\pm 60^\circ$). Note that all synthesized results of SI SF-GAN are consistent with the ground-truth (GT) faces, showing clear superiority across the different pose and lighting variations. Moreover, MI SF-GAN further improves the image quality of the synthesized images, while preserving the identity even better than SI SF-GAN.

4.3. Identity preserving property

To quantitatively demonstrate the identity preserving ability of proposed SF-GAN, we evaluate face recognition

²<https://github.com/HRLTY/TP-GAN>.

³<https://github.com/bluer555/CR-GAN>.

⁴<https://github.com/yulunzhang/RCAN>.

Table 1: **Multi-PIE Setting 2.** PSNR (dB), SSIM and Rank-1 (%) performance across views (α). SI SF-GAN on LR input can recover even better identity information and finer detail than the state-of-the-art methods trained on super-resolved input.

	α	PSNR					SSIM					Rank - 1				
		$\pm 60^\circ$	$\pm 45^\circ$	$\pm 30^\circ$	$\pm 15^\circ$	Avg	$\pm 60^\circ$	$\pm 45^\circ$	$\pm 30^\circ$	$\pm 15^\circ$	Avg	$\pm 60^\circ$	$\pm 45^\circ$	$\pm 30^\circ$	$\pm 15^\circ$	Avg
TP-GAN [16]	LR	19.00	19.22	19.52	19.67	19.35	0.625	0.634	0.645	0.654	0.640	57.87	65.78	69.13	73.99	66.69
	SR	19.06	19.32	19.55	19.69	19.41	0.638	0.647	0.657	0.664	0.652	68.95	77.58	81.69	84.83	78.26
CR-GAN [33]	LR	16.83	18.04	18.03	18.76	17.92	0.499	0.536	0.548	0.567	0.538	46.89	57.53	60.93	65.54	57.72
	SR	19.53	19.71	19.92	20.20	19.84	0.632	0.640	0.648	0.653	0.643	67.45	70.63	71.44	71.99	70.38
FNM [26]	LR	15.50	15.79	16.32	17.25	16.22	0.433	0.439	0.451	0.470	0.448	62.68	66.54	69.22	72.31	67.69
	SR	15.58	16.00	16.72	17.61	16.48	0.427	0.436	0.449	0.468	0.445	76.21	79.46	82.08	85.05	80.7
M2FPA [22]	LR	22.38	22.73	23.17	23.91	23.05	0.692	0.704	0.719	0.743	0.715	66.50	76.95	84.24	90.52	79.55
	SR	22.48	22.82	23.29	24.11	23.18	0.697	0.710	0.728	0.755	0.723	79.32	88.03	93.35	97.63	89.58
SI SF-GAN	LR	22.58	23.02	23.56	24.53	23.42	0.700	0.717	0.736	0.764	0.729	85.25	92.31	95.85	97.82	92.81

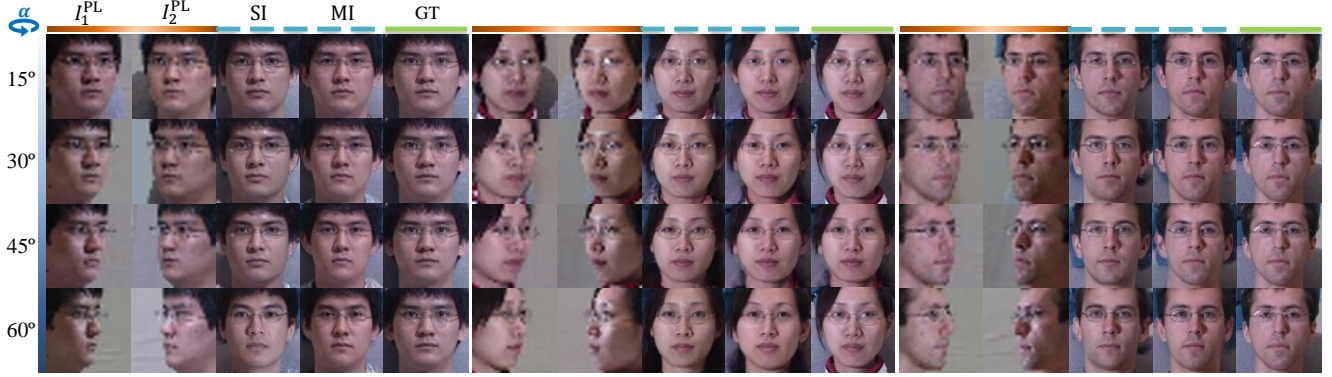


Figure 5: **SI and MI SF-GAN synthesis results.** SI SSF-GAN recovers better frontal faces than existing methods for different yaws (α) (Fig. 4). However, MI SF-GAN further improves the image quality and identity preserving ability.

Table 2: **CAS-PEAL-R1.** Rank-1 recognition performance (%) across pitches (β).

β		-15°	0°	$+15^\circ$
	LR	90.97	94.96	91.01
TP-GAN [16]	SR	94.08	97.70	94.50
	LR	72.86	87.92	78.94
CR-GAN [33]	SR	79.51	89.80	84.45
	LR	94.36	98.21	96.32
M2FPA [22]	SR	97.91	99.35	98.74
	LR	98.06	99.88	98.87

accuracy on synthesized frontal images. Table 1 compares face recognition performance with existing state-of-the-art on setting 2 of Multi-PIE across different poses. Results on setting 1 of Multi-PIE are shown in the supplementary material. Results are reported with Rank-1 recognition accuracy. We conduct the experiment by extracting features using a pre-trained face recognition model (*i.e.* 29-layer Light-CNN[36]), and then compute feature similarities via cosine-distance metric. Results on setting 2 of Multi-PIE shows that SF-GAN consistently achieves the best performance across all angles. Note that the existing methods tend to fail capturing identity information from LR input, while

the performance is largely improved with a two-step processing, which is to first super-resolve the side-view faces and then frontalize them. However, the proposed SF-GAN can recover identity preserving and HR frontal faces directly from LR images, and have even better performance than the SOTA methods trained with SR images.

We analyze, quantitatively, the benefits of using the proposed in the LFW benchmark (Table 3). Specifically, face recognition performance is evaluated on synthesized frontal images. The results of SOTA are in Table 3 are from [22]. Similarly, we show the rank-1 recognition accuracy for CAS-PEAL-R1 across pitch (β) pose variations. The quantitative results are summarized in Table 2, which demonstrates that SF-GAN significantly outperforms its competitors in terms of identity preservation.

To the best of our knowledge, only DR-GAN [34] attempted to solve the MI frontal face problem. We follow the settings in [34] for MI fusion. First, a subset \mathbb{P}_0 of images with poses in (30° , 60°) is selected from the Multi-PIE probe set. Then, we form four probe sets $\{\mathbb{P}_i\}_{i=1}^4$ with the image count ranging from 1-to-4. Specifically, \mathbb{P}_1 is formed by randomly selecting one image per subject from \mathbb{P}_0 . \mathbb{P}_2 is formed by adding a random image per subject to \mathbb{P}_1 . Similarly, \mathbb{P}_3 and \mathbb{P}_4 are constructed. For face recogni-

Table 3: **LFW benchmark.** Face verification accuracy (ACC) and area-under-curve (AUC) results.

	ACC (%)	AUC (%)
LFW-3D [11]	93.62	88.36
LFW-HPEN [44]	96.25	99.39
FF-GAN [39]	96.42	99.45
CAPG-GAN [13]	99.37	99.90
M ² FPA [22]	99.41	99.92
FNM [26]	99.42	99.93
Ours	99.48	99.96

Table 4: **Ablation Study of SI and MI SF-GAN.** Average Rank-1 (%), PSNR (dB) and SSIM on MutiPIE setting 2.

		Rank-1	PSNR	SSIM
SI	baseline_1	84.99	23.21	0.718
	baseline_2	91.34	23.38	0.724
	w/o L1 (pixel)	90.81	23.34	0.730
	w/o SSIM (patch)	91.16	23.29	0.727
	w/o ID (global)	81.49	23.32	0.726
	w/o Adv (global)	91.81	23.87	0.758
	SF-GAN	92.81	23.42	0.729
MI	image-level	96.09	23.98	0.755
	feat-level	97.68	24.21	0.760
	SF-GAN	98.43	24.43	0.762

tion, we directly obtained results reported in the DR-GAN paper, since we fail training the model on LR and SR images. Note that results for DR-GAN are trained and tested on HR images, with ours outperforming most (Table 5).

4.4. Ablation study

We conduct an ablation study as a deep-dive revealing the benefits of the SR-integrated architecture, the different synthesis loss function, and the multi-view fusion method.

Effect of SR side-view module. To highlight the importance of *SR side-view*, we compare SF-GAN with and without the SR module (Table 4). Specifically, we remove the SR module (*i.e.* *baseline_1*). Then, the same structure as SF-GAN except with no supervision for *SR side-view* (*i.e.* *baseline_2*). We use Rank-1, PSNR and SSIM to evaluate. Results show *baseline_1* performs the poorest, implying the second branch learns complimentary features even without supervision. Hence, the added high-frequency information for frontal face synthesis persists. Moreover, the performance is further improved with a supervised *SR side-view*, validating the contributions of this module.

Effect of different losses. We show the contribution of each type of loss by removing one of the three losses, pixel- (*i.e.* L_1), patch- (*i.e.* L_{SSIM}), or global- (*i.e.* L_{ID} , L_{Adv}) (Table 4). Rank-1 recognition accuracy, PSNR, and SSIM of frontalized images are used for evaluation. The qualitative results are shown in the supplementary material. We observe the recognition performance sharply decreases with

Table 5: **MI performance.** Rank-1 recognition performance (%) of different fusion scheme (*i.e.* image-level, feature-level, and with the proposed constraint in G).

# of images	1	2	3	4
DR-GAN [34]	85.90	92.80	95.10	96.00
image-level	91.14	87.14	90.71	93.69
feat-level	91.14	92.01	96.80	99.03
+constraints	91.14	92.74	96.97	99.19

the global and without the pixel. Though the PSNR and SSIM is largely improved without L_{Adv} , the synthesized images tend to be blurry without L_{Adv} . Comparing results between patch (L_{SSIM}) and pixel-level (L_1) loss, we observed that recognition accuracy is higher without L_{SSIM} , while PSNR and SSIM are higher without L_1 . With both loss, the proposed SF-GAN achieves the best in terms of Rank-1 and PSNR, and comparable in SSIM (only 0.001 lower), implying that L_{SSIM} and L_1 are complimentary.

Effect of fusion scheme via orthogonal constrain. We gain insight by exploring various fusion methods. We conduct two experiments to validate the proposed fusion scheme: (1) fuse two LR images with opposite poses α and $-\alpha$ (Table 4), and (2) fuse MI with arbitrary poses spanning $[30^\circ, 60^\circ]$ (Table 5). For MI fusion, we follow the experiment setting of DR-GAN (Section 4.3). We compare Rank-1 recognition accuracy and PSNR of synthesized images for both. The results demonstrate that more inputs improve identity preservation when fused in image or feature space. Moreover, we gain further improvement by adding orthogonal constraints to penalize redundant latent representations and diversify the features.

5. Conclusion

We proposed SuperFront generative adversarial network (SF-GAN) to synthesize photo-realistic, identity-preserving frontal faces from LR-to-HR. To the best of our knowledge, we are the first to address the problem of rotating tiny profile faces. Our *SR side-view* module enhances faces to provide the high-frequency details needed to produce high-quality, identity-preserving faces. In parallel to this, we introduce a patch loss that captures facial structure information and complements pixel loss. With the two modules fused, a precise non-linear mapping between LR side-view and HR frontal-view is learned. Furthermore, the proposed model handles single and multi-image inputs—more samples with arbitrary poses per subject as input, the better the quality of the synthesized output. A constraint is imposed on multi-image inputs to remove redundant information (*i.e.* orthogonal regularization). We explore different fusion techniques, providing an ablation study to characterize our model in a complete, transparent manner. Quantitative and qualitative results demonstrate SF-GAN as state-of-the-art.

References

- [1] Akshay Asthana, Tim K Marks, Michael J Jones, Kinh H Tieu, and MV Rohith. Fully automatic pose-invariant face recognition via 3d pose normalization. pages 937–944. IEEE, 2011. 2
- [2] N. Bansal, X. Chen, and Z. Wang. Can We Gain More from Orthogonality Regularizations in Training Deep CNNs? *arXiv preprint arXiv:1810.09102*, Oct. 2018. 2, 3
- [3] Adrian Bulat and Georgios Tzimiropoulos. Super-fan: Integrated facial landmark localization and sr of real-world low resolution faces in arbitrary poses with gans. In *CVPR*, 2018. 1
- [4] Yu Chen, Ying Tai, Xiaoming Liu, Chunhua Shen, and Jian Yang. Fsrnet: End-to-end learning face sr with facial priors. In *CVPR*, 2018. 1
- [5] Yunje Choi, Minje Choi, Munyoung Kim, Jung-Woo Ha, Sunghun Kim, and Jaegul Choo. Stargan: Unified generative adversarial networks for multi-domain image-to-image translation. In *CVPR*, 2018. 1
- [6] Jeff Donahue, Philipp Krähenbühl, and Trevor Darrell. Adversarial feature learning. *arXiv preprint arXiv:1605.09782*, 2016. 2
- [7] Wen Gao, Bo Cao, Shiguang Shan, Xilin Chen, Delong Zhou, Xiaohua Zhang, and Debin Zhao. The cas-peal large-scale chinese face database and baseline evaluations. *IEEE Transactions on Systems, Man, and Cybernetics-Part A: Systems and Humans*, 2007. 5
- [8] Ian Goodfellow, Jean Pouget-Abadie, Mehdi Mirza, Bing Xu, David Warde-Farley, Sherjil Ozair, Aaron Courville, and Yoshua Bengio. Generative adversarial nets. pages 2672–2680, 2014. 2
- [9] Ralph Gross, Iain Matthews, Jeffrey Cohn, Takeo Kanade, and Simon Baker. Multi-pie. *Image and Vision Computing*, 2010. 5
- [10] Yandong Guo, Lei Zhang, Yuxiao Hu, Xiaodong He, and Jianfeng Gao. Ms-celeb-1m: A dataset and benchmark for large-scale face recognition. 2016. 6
- [11] Tal Hassner, Shai Harel, Eran Paz, and Roei Enbar. Effective face frontalization in unconstrained images. In *CVPR*, 2015. 6, 8
- [12] Zhenliang He, Wangmeng Zuo, Meina Kan, Shiguang Shan, and Xilin Chen. Attgan: Facial attribute editing by only changing what you want. *IEEE Transactions on Image Processing*, 2019. 1
- [13] Yibo Hu, Xiang Wu, Bing Yu, Ran He, and Zhenan Sun. Pose-guided photorealistic face rotation. In *CVPR*, 2018. 1, 5, 8
- [14] Gary B Huang, Marwan Mattar, Tamara Berg, and Eric Learned-Miller. Labeled faces in the wild: A database for studying face recognition in unconstrained environments. 2008. 6
- [15] Gary B. Huang, Manu Ramesh, Tamara Berg, and Erik Learned-Miller. Labeled faces in the wild: A database for studying face recognition in unconstrained environments. Technical report, University of Massachusetts, Amherst, 2007. 5
- [16] Rui Huang, Shu Zhang, Tianyu Li, and Ran He. Beyond face rotation: Global and local perception gan for photorealistic and identity preserving front view synthesis. 2017. 1, 2, 5, 6, 7
- [17] Phillip Isola, Jun-Yan Zhu, Tinghui Zhou, and Alexei A Efros. Image-to-image translation with conditional adversarial networks. In *CVPR*, 2017. 2
- [18] Justin Johnson, Alexandre Alahi, and Li Fei-Fei. Perceptual losses for real-time style transfer and super-resolution. 2016. 5
- [19] Meina Kan, Shiguang Shan, Hong Chang, and Xilin Chen. Stacked progressive auto-encoders (spae) for face recognition across poses. pages 1883–1890, 2014. 2
- [20] Paul Koppen, Zhen-Hua Feng, Josef Kittler, Muhammad Awais, William Christmas, Xiao-Jun Wu, and He-Feng Yin. Gaussian mixture 3d morphable face model. *Pattern Recognition*, 74:617–628, 2018. 2
- [21] Christian Ledig, Lucas Theis, Ferenc Huszár, Jose Caballero, Andrew Cunningham, Alejandro Acosta, Andrew Aitken, Alykhan Tejani, Johannes Totz, Zehan Wang, et al. Photorealistic single image super-resolution using a generative adversarial network. In *CVPR*, 2017. 2
- [22] Peipei Li, Xiang Wu, Yibo Hu, Ran He, and Zhenan Sun. M2fpa: A multi-yaw multi-pitch high-quality database and benchmark for facial pose analysis. 2019. 1, 2, 3, 4, 5, 6, 7, 8
- [23] Shaoxin Li, Xin Liu, Xiujuan Chai, Haihong Zhang, Shihong Lao, and Shiguang Shan. Morphable displacement field based image matching for face recognition across pose. pages 102–115. Springer, 2012. 2
- [24] Sifei Liu, Jimei Yang, Chang Huang, and Ming-Hsuan Yang. Multi-objective convolutional learning for face labeling. 2015. 4
- [25] Deepak Pathak, Philipp Krahenbuhl, Jeff Donahue, Trevor Darrell, and Alexei A Efros. Context encoders: Feature learning by inpainting. In *CVPR*, 2016. 2
- [26] Yichen Qian, Weihong Deng, and Jiani Hu. Unsupervised face normalization with extreme pose and expression in the wild. In *Proceedings of the IEEE Conference on Computer Vision and Pattern Recognition*, pages 9851–9858, 2019. 1, 6, 7, 8
- [27] Xuebin Qin, Zichen Zhang, Chenyang Huang, Chao Gao, Masood Dehghan, and Martin Jagersand. Basnet: Boundary-aware salient object detection. In *CVPR*, 2019. 2
- [28] Viswanath K Reddy and Shruthi B Gangal. Concatenation of multiple features for face recognition. In *International Conference on Smart Trends for Information Technology and Computer Communications*, pages 558–564. Springer, 2016. 2
- [29] Olaf Ronneberger, Philipp Fischer, and Thomas Brox. U-net: Convolutional networks for biomedical image segmentation. In *The Medical Image Computing and Computer Assisted Intervention Society*, 2015. 2, 4
- [30] Christos Sagonas, Yannis Panagakis, Stefanos Zafeiriou, and Maja Pantic. Robust statistical face frontalization. pages 3871–3879, 2015. 2

- [31] Wenzhe Shi, Jose Caballero, Ferenc Huszár, Johannes Totz, Andrew P Aitken, Rob Bishop, Daniel Rueckert, and Zehan Wang. Real-time single image and video super-resolution using an efficient sub-pixel convolutional neural network. 2016. [4](#)
- [32] Yifan Sun, Liang Zheng, Weijian Deng, and Shengjin Wang. Svdnet for pedestrian retrieval. pages 3800–3808, 2017. [3](#)
- [33] Yu Tian, Xi Peng, Long Zhao, Shaoting Zhang, and Dimitris N Metaxas. Cr-gan: learning complete representations for multi-view generation. 2018. [2](#), [6](#), [7](#)
- [34] Luan Tran, Xi Yin, and Xiaoming Liu. Disentangled representation learning gan for pose-invariant face recognition. 2017. [1](#), [2](#), [7](#), [8](#)
- [35] Zhou Wang, Alan C Bovik, Hamid R Sheikh, Eero P Simoncelli, et al. Image quality assessment: from error visibility to structural similarity. 13(4):600–612, 2004. [2](#), [4](#)
- [36] Xiang Wu, Ran He, Zhenan Sun, and Tieniu Tan. A light cnn for deep face representation with noisy labels. *IEEE Transactions on Information Forensics & Security*, 2018. [4](#), [7](#)
- [37] Di Xie, Jiang Xiong, and Shiliang Pu. All you need is beyond a good init: Exploring better solution for training extremely deep convolutional neural networks with orthonormality and modulation. 2017. [3](#)
- [38] Junho Yim, Heechul Jung, ByungIn Yoo, Changkyu Choi, Dusik Park, and Junmo Kim. Rotating your face using multi-task deep neural network. 2015. [5](#)
- [39] Xi Yin, Xiang Yu, Kihyuk Sohn, Xiaoming Liu, and Manmohan Chandraker. Towards large-pose face frontalization in the wild. 2017. [1](#), [2](#), [3](#), [8](#)
- [40] Yu Yin, Songyao Jiang, Joseph P. Robinson, and Yun Fu. Dual-attention gan for large-pose face frontalization, 2020. [1](#)
- [41] Yu Yin, Joseph P Robinson, Yulun Zhang, and Yun Fu. Joint super-resolution and alignment of tiny faces. 2020. [1](#)
- [42] Yulun Zhang, Kunpeng Li, Kai Li, Lichen Wang, Bineng Zhong, and Yun Fu. Image super-resolution using very deep residual channel attention networks. In *Proceedings of the European Conference on Computer Vision (ECCV)*, pages 286–301, 2018. [6](#)
- [43] Yulun Zhang, Yapeng Tian, Yu Kong, Bineng Zhong, and Yun Fu. Residual dense network for image super-resolution. pages 2472–2481, 2018. [4](#)
- [44] Xiangyu Zhu, Zhen Lei, Junjie Yan, Dong Yi, and Stan Z Li. High-fidelity pose and expression normalization for face recognition in the wild. 2015. [2](#), [6](#), [8](#)
- [45] Zhenyao Zhu, Ping Luo, Xiaogang Wang, and Xiaoou Tang. Deep learning identity-preserving face space. pages 113–120, 2013. [2](#)
- [46] Zhenyao Zhu, Ping Luo, Xiaogang Wang, and Xiaoou Tang. Multi-view perceptron: a deep model for learning face identity and view representations. pages 217–225, 2014. [2](#)